Shock tube ignition delay times and methane time-histories measurements during excess CO_2 diluted oxy-methane combustion

*Batikan Koroglu, Owen M. Pryor, Joseph Lopez, Leigh Nash, Subith S. Vasu**

Center for Advanced Turbomachinery and Energy Research, Mechanical and Aerospace Engineering, University of Central Florida, Orlando, FL 32816

***Corresponding Email:** subith@ucf.edu

Abstract

The combustion of methane in air results in large amounts of CO_2 and NO_X emissions. In order to reduce the NO_X emissions, one possible solution is the oxy-methane combustion with large CO_2 dilution so that the combustion products can be reduced mainly to CO_2 and H_2O. However, there are very few studies on the chemical kinetics of oxy-methane combustion in a CO_2 diluted environment. In this study, methane time-histories, CH* emission profiles, and pressure time-histories measurements were conducted behind reflected shock waves to gain insight into the effects of CO_2 dilution of the gas mixtures on the ignition of methane. The measurements were carried out for mixtures of CH_4, CO_2 and O_2 in argon bath gas at temperatures of 1577-2144 K, pressures of 0.53-4.4 atm, equivalence ratios (Φ) of 0.5, 1, and 2, and CO_2 mole fractions (X_{CO2}) of 0, 30%, and 60%. The laser absorption measurements were conducted using a continuous wave distributed feedback interband cascade laser (DFB ICL) centered at 3403.4 nm. The results showed the decrease of activation energy and the increase of ignition delay time as the amount of CO_2 dilution was increased. However, the changes were minor and within the experimental uncertainties of the measurements. Also, the results were compared to the predictions of two different natural gas mechanisms: GRI 3.0 and AramcoMech 1.3 mechanisms. In general the predictions were reasonable when compared to the experimental data; however, there were discrepancies at some conditions. Three different influences of CO_2 addition to the argon bath gas in regards to chemistry, collision efficiencies, and heat capacities were examined. In addition, the present study included experimentally obtained correlations for absorption cross sections of methane for its P(8) line in the v_3 band in argon bath gas with and without carbon-dioxide dilutions at temperatures between $1200 < T < 2000$ K and pressures between $0.7 < P < 1.2$ atm.

1. INTRODUCTION

Energy consumption has increased dramatically as the world advances and becomes more industrialized. Over the next twenty five years, the U.S. Department of Energy expects the energy demand to increase by 29% with almost all of the new energy from natural gas [1]. A problem is that current methods for the combustion of natural gas (e.g., gas turbines) result in large amounts of CO_2 and NO_X emissions. In order to reduce the greenhouse gases, one possible solution is the oxy-methane

combustion with large CO_2 dilution. By using pure oxygen instead of air, the resulting products can be reduced to mainly CO_2 and H_2O. H_2O can be condensed out and remaining CO_2 can then be captured and returned to the power cycle or stored underground. The concern is the difference in methane oxidation in air vs CO_2 mixtures. It has been shown that the reactions behave differently as the properties of nitrogen and carbon dioxide differ [2] in terms of participation in combustion reactions directly or as a third-body collision partner. As a result, more analysis of oxy-methane combustion with high CO_2 addition needs to be conducted.

There are some studies of CO_2 diluted oxy-methane combustion in the literature. Heil et al. investigated the methane burning rates for flameless combustion and compared the results to nitrogen diluted mixtures [3]. Di Benedetto et al. and Liu et al. looked at the chemical effects (flammability and burning velocity) of methane combustion in CO_2 versus N_2 [4, 5]. The laminar flame speeds have also been studied for various conditions [6-9]. In addition, Vasu et al. examined the effect of CO_2 dilution on the ignition delay times of syngas mixtures of hydrogen and carbon monoxide [10]. However, there are very few studies in the literature that probed the effects of excess CO_2 dilution on the ignition delay times of methane. Holton et al. conducted ignition delay time measurements of natural gas blends, including methane and ethane mixtures, with small amounts of CO_2 addition (5 and 10%) [11]. They found out that methane and ethane blends at $\Phi = 0.5$ and T=1137 K diluted with 5% CO_2 increased the ignition delay time by only 2%, whereas 10% CO_2 addition to the same mixture resulted in longer times by 46% . This increase was attributed to the third-body collision efficiencies of CO_2 being an order of magnitude greater than those of N_2. However, they suggested carrying out further experiments in order to better quantify the effect of CO_2 addition on the ignition delay time.

Figure 1 (a) gives the comparison of methane time-history predictions of two different reaction mechanisms; namely the GRI 3.0 and the AramcoMech 1.3 [12, 13], for stoichiometric combustion of 3.5% CH_4 in argon bath gas diluted with 30% CO_2 at 1600K and 1 atm. The results were obtained using the constant- volume, internal energy (constant-U,V) assumption with the CHEMKIN PRO tool [14]. The discrepancy in the ignition delay time between the two mechanisms turned out to be $\Delta\tau_{ign}$ = 462.5 μs. Fig. 1 (b) shows CH_4 time-histories during its ignition when the gas mixture contains different mole fractions of CO_2 ranging from 0 up to 60% according to the simulations done with the AramcoMech 1.3 mechanism. The differences in the ignition delay times were $\Delta\tau_{ign}$ = 293 and 236 μec when X_{CO2} was increased from 0 to 0.3 and 0.3 to 0.6, respectively. These variations in the predictions of two chemical mechanisms with the addition of CO_2 necessitate conducting validation experiments on CH_4 ignition with CO_2 dilution.

a)

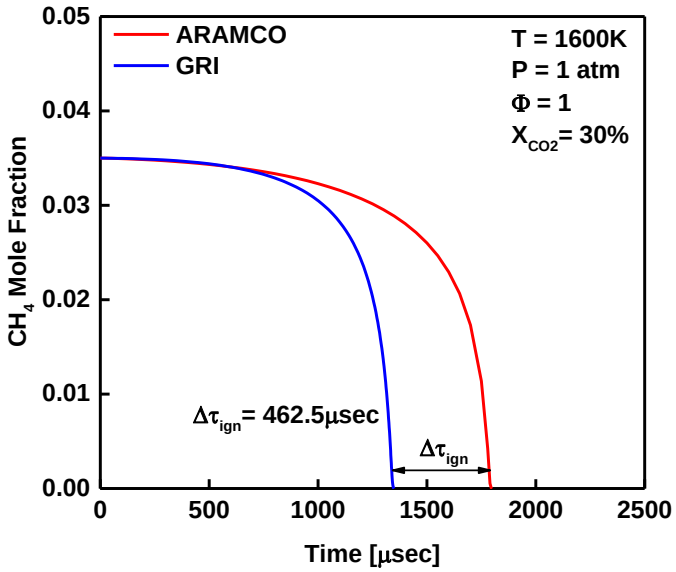

b)

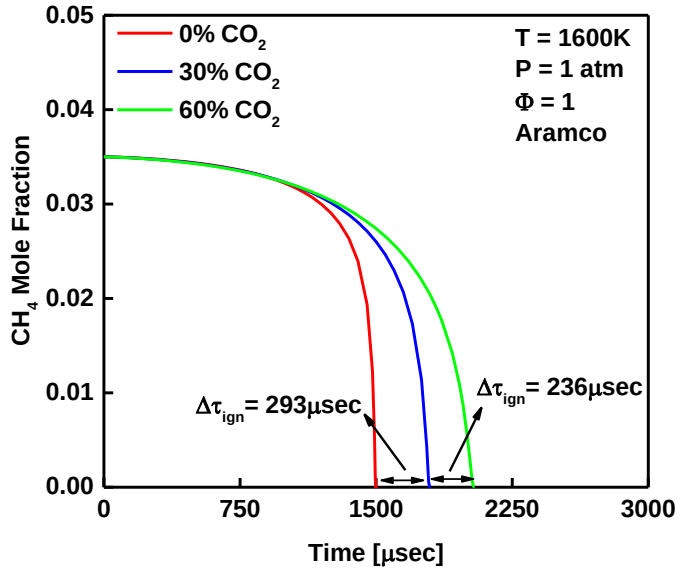

Figure 1 (a) Comparison of methane time-history predictions obtained from GRI 3.0 and AramcoMech 1.3 mechanisms for the stoichiometric combustion of 3.5% CH_4 in 30% CO_2 in argon bath gas at 1600K and 1 atm; **(b)** methane time-histories during its ignition when the bath gas contains different percentages of CO_2 ranging from 0 up to 60% according to the AramcoMech 1.3 mechanism. Note: The reader is referred to the online version of this article for better color clarity for all figures.

Although not shown in Figs. 1(a) and (b), the discrepancies in the predicted ignition delay times between the two mechanisms were noticed in N_2 and Ar bath gas even without any CO_2 dilution. These ignition delay time simulations at different bath gasses and CO_2 dilutions at 1600 K and 1 atm are summarized in Table 1. It can be seen from the table that as the CO_2 dilution was increased from 0 to

60%, the differences ($\Delta\tau_{dif}$) between the two mechanisms raised from 405.5 μs to 477.5 μs in argon bath. However, the difference between the two mechanisms remained the same (499.4 μs < $\Delta\tau_{dif}$ < 503.3 μs) when nitrogen was used as the bath gas. Also, differences in the ignition delay times within the mechanisms themselves were seen as the CO_2 dilution was raised. This was already exemplified in Fig. 1 (b), but further detailed in Table 1. As the CO_2 amount was increased, it was observed that the changes in the ignition delay time were more significant when the bath gas included argon (e.g. an increase from 1495.5 to 2024.9 μs for AramcoMech 1.3 mechanism) than nitrogen (e.g. an increase from 1665.8 to 2059.4 μs for AramcoMech 1.3 mechanism).

Table 1 Ignition Delay Time Simulation Predictions at 1600 K and 1 atm

	X_{AR}	X_{N2}	X_{CH4}	X_{O2}	X_{CO2}	$\tau_{AramcoMech\ 1.3}$ [μs]	$\tau_{GRI\ 3.0}$ [μs]	$\Delta\tau_{dif}$
Ar bath	0.895	0	0.035	0.07	0	1495.5	1090.1	405.5
	0.595	0			0.3	1788.3	1325.8	462.5
	0.295	0			0.6	2024.9	1547.4	477.5
N_2 bath	0	0.895	0.035	0.07	0	1665.8	1164.8	501.0
	0	0.595			0.3	1865.8	1362.5	503.3
	0	0.295			0.6	2059.4	1560.0	499.4

In this study we provided ignition delay time measurements for mixtures of CH_4, CO_2, and O_2 in argon bath gas at temperatures of 1577-2144 K, pressures of 0.53-4.4 atm, equivalence ratios (Φ) of 0.5, 1, and 2, and CO_2 mole fractions (X_{CO2}) of 0, 0.3, and 0.6. The measurements were done by utilizing a recently built shock tube facility at the University of Central Florida (UCF) in the reflected shock region. Experimental data were compared to the predictions of two different kinetic models: GRI 3.0 and AramcoMech 1.3 mechanisms [12, 13]. The ignition delay time measurements showed the influence of CO_2 dilution on the oxidation of methane. In addition, we built a laser absorption diagnostic for measuring CH_4 time-histories behind the reflected shock waves using a continuous wave distributed feedback interband cascade laser (DFB ICL) centered at 3403.4 nm. The present study included experimentally obtained correlations for absorption cross sections of CH_4 for its P(8) line in the v_3 band (λ = 3403.4 nm) in argon bath gas with (X_{CO2} = 0.3) and without (X_{CO2} = 0.0) CO_2 dilutions at temperatures of 1200 < T < 2000 K and pressures of 0.7 < P < 1.2 atm. CH_4 time-histories during stoichiometric ignition of CH_4 with and without CO_2 dilution around 1 atm were also obtained through the aforementioned absorption cross section correlations. To the best of our knowledge, the current study provides the first shock tube measurements of ignition times and CH_4 time-histories in methane combustion with excess CO_2 dilution (≥ 30%) in argon.

2. EXPERIMENTAL SETUP AND PROCEDURE

The procedure for shock tube and laser experiments are similar to those adopted in current author's previous work at Stanford [10, 15-21] and is briefly discussed here.

2.1 Shock Tube Facility

A stainless steel shock tube was built by means of six pipes with inside and outside diameters of 14.17 and 16.80 cm, respectively. The driver and driven sections lengths were 4.88 and 8.54 m, respectively. A diaphragm separated these two regions and a normal shock wave was created through the sudden rupture of it by means of an in-house manufactured cutter. Two different test pressures (~1 and 4 atm) were obtained by using two different thicknesses (0.127 and 0.508 mm) of polycarbonate lexan diaphragms (Regal Plastics). The test section of the shock tube had 8 optical ports located 2 cm away from the end wall of the driven section. One port was installed with a piezoelectric pressure transducer (Kistler 603B1) to measure the pressure in the reflected shock region. Sapphire windows of 19.05 mm diameter and 3 mm thickness (Meller Optics) were flush mounted also at the same location for line of sight laser absorption as well as emission measurements. An 8 channel data acquisition board (NI PCI-6133; 2.5M Samples/second/channel) was used for the measurements of pressure, emission, and concentration versus time-histories.

Five piezoelectric pressure transducers (PCB 113B26; 500 kHz frequency response) connected to four time-interval counters (Agilent 53220A; 0.1 ns time resolution) were placed along the last 1.4 m of the shock tube to monitor the normal shock wave passage and thus to measure the incident shock velocities, which were then linearly extrapolated to the end wall. The temperature (T) and pressure (P) in the reflected shock region were calculated based on the extrapolated end wall shock velocity, initial temperature and pressure in the driven section by using one dimensional ideal shock relations [22] and assuming chemically frozen and vibrationally equilibrated gasses. The incident shock wave attenuation was always found to be less than 1%. The uncertainty in the reflected shock temperature and pressure were estimated to be less than ±1 %.

2.2 Fuel/oxidizer Mixture Preparation

Before mixture preparation and shock tests, the shock tube and the mixing facility were vacuumed by a turbo molecular pump system (Agilent model V301) together with three rotary vane pumps (Agilent DS102). The vacuum pressure was measured by convection (Lesker KJL275804LL) and ionization (Lesker KJLC354401YF) gauges operating between $1x10^{-4}$ and 1000 Torr and between $1x10^{-9}$ and $5x10^{-2}$ Torr, respectively. Before any experiment was conducted, the pressure of the shock tube setup was brought to $1x10^{-5}$ Torr, which typically occurred within an hour.

The test gases for the experiments were prepared in a 0.033 m^3 teflon-coated stainless steel high purity mixing facility. Different mixtures were created manometrically and then mixed overnight with a magnetically driven stirrer to ensure homogeneity. Pressures were measured using a 100 Torr (MKS Instruments/Baratron E27D, accuracy of 0.12% of reading) and 10,000 Torr (MKS Instruments/Baratron 628D, accuracy of 0.25% of reading) full scale range capacitance manometers. Research grade argon (99.999%), oxygen (99.999%), carbon dioxide (99.999%), and methane (99.99%) were supplied by Air Liquide. The prepared test mixtures were introduced into the electro-polished driven section of the shock tube before the experiments were conducted.

2.3 Ignition Delay Time Measurements

The ignition delay time was defined as the time interval between the arrival of the reflected shockwave and the onset of ignition at the measurement location (2 cm away from the end wall), which were determined from the pressure (or laser schlieren spikes) and emission measurements, respectively. The emissions were measured using a GaP transimpedance amplified detector (Thorlabs PDA25K) operating in the wavelength range between 150 and 550 nm. A band pass filter at 430 ±2 nm (Thorlabs FB430-10) for detecting the ($A^2\Delta$-$X^2\Pi$) transitions of the CH* radical was placed between a variable Slit (Thorlabs VA100/M) and the detector. The slit size was set to 1mm aperture for achieving adequate time resolution. The onset of ignition from the CH* emission history was determined by finding the time of steepest rise and linearly extrapolating back in time to the pre-ignition baseline. This method was already described in a previous study of Vasu et al. [23]. The uncertainties in the ignition delay time measurements were estimated to be between ±12 and ±18% depending on the test conditions.

2.4 CH_4 Time-Histories Measurements

A continuous wave distributed feedback inter-band cascade laser (Nanoplus DFB ICL) was set up and used for measuring methane (CH_4) concentration time-histories during methane's ignition with and without CO_2 dilution. The wavelength was chosen as 3403.4 nm as it coincides with methane's P(8) line in its v_3 band [24]. Since the laser has 4 nm tuning range, this setup is used in our lab for the interference-free detection of methane concentration time-histories during higher hydrocarbon combustion pyrolysis and oxidation, which is achieved via a peak-minus-valley absorption scheme, because it has been clearly indicated in Pyun et al. [25-27] that many hydrocarbons have constant absorption cross section in the close vicinity of 3403.4 nm.

Figure 2 shows the schematic of the end section of the shock tube with the laser and optical components. The laser diode was collimated using a lens (Thorlabs C036TMEE) and a laser beam profiler (Spiricon Pyrocam-III). The laser diode was mounted on a heat sink (Nanoplus TO66 mount) which was also connected to temperature (Thorlabs TLD001) and injection current (Thorlabs TTC001) controllers.

The laser beam was split into two parts; a reference beam (I_{ref}) and the transmitted light (I_{tr}) that passed through the shock tube. Each beam was incident on a focusing mirror (Thorlabs CM254-050-P01) and a thermoelectrically cooled HgCdTe (MCT) detector (Vigo Systems PVI-2TE-3.4). The transmitted beam was passed through aan iris (Thorlabs ID25), neutral density filter (Thorlabs NDIR10A), and band pass filter (Thorlabs FB3500-500) to attenuate and minimize the interference on the detectors due to the emission of gas species at high temperatures.

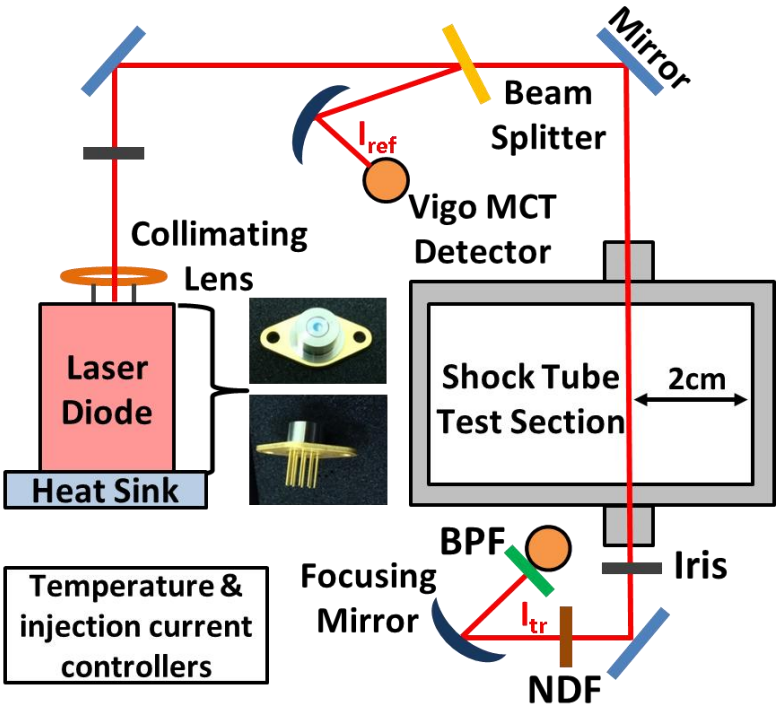

Figure 2 The schematic of the end section of the shock tube with the laser and the optical components.

The ratio of the transmitted and reference light intensities (I_{tr}/I_{ref}) were measured in order to obtain CH_4 mole fraction from Beer-Lambert law given by

$$-\ln\left(\frac{I_{tr}}{I_{ref}}\right)_{\nu} = \sigma(\nu,T,P)\frac{P_{tot}}{RT}\chi L \qquad (1)$$

where P [atm] is the pressure and T [K] is the temperature of the gas; L[cm] is the optical path length; σ [cm^2/molecule] is the absorption cross section; and χ is the mole fraction of the absorbing species (CH_4).

Figure 3 (a) shows the prediction results for the main products of ignition of stoichiometric methane and oxygen mixture (3.5% CH_4 and 7% O_2) in argon bath gas at 1600 K and 1 atm. The results were obtained from the AramcoMech 1.3 mechanism using CHEMKIN PRO simulations. Figure 3 (b) displays the absorption cross section of these main combustion products as well as that of methane around 3403.4 nm at 296K and 1 atm. It can be clearly seen that the main products have no or almost negligible

absorption features around this wavelength region. Therefore, the measurements of the current study were done only at this peak wavelength (3403.4 nm). Note that these absorption cross section values were taken from the HITRAN database. Since the conditions behind the reflected shock wave (T_5 and P_5) are different for ignition experiments, measurements of the absorption cross section of methane at elevated temperatures were carried out. These measurements were done with a non-reactive gas mixture involving 2% methane in argon bath gas with (X_{CO2} = 0.3) and without (X_{CO2} = 0.0) CO_2 dilutions.

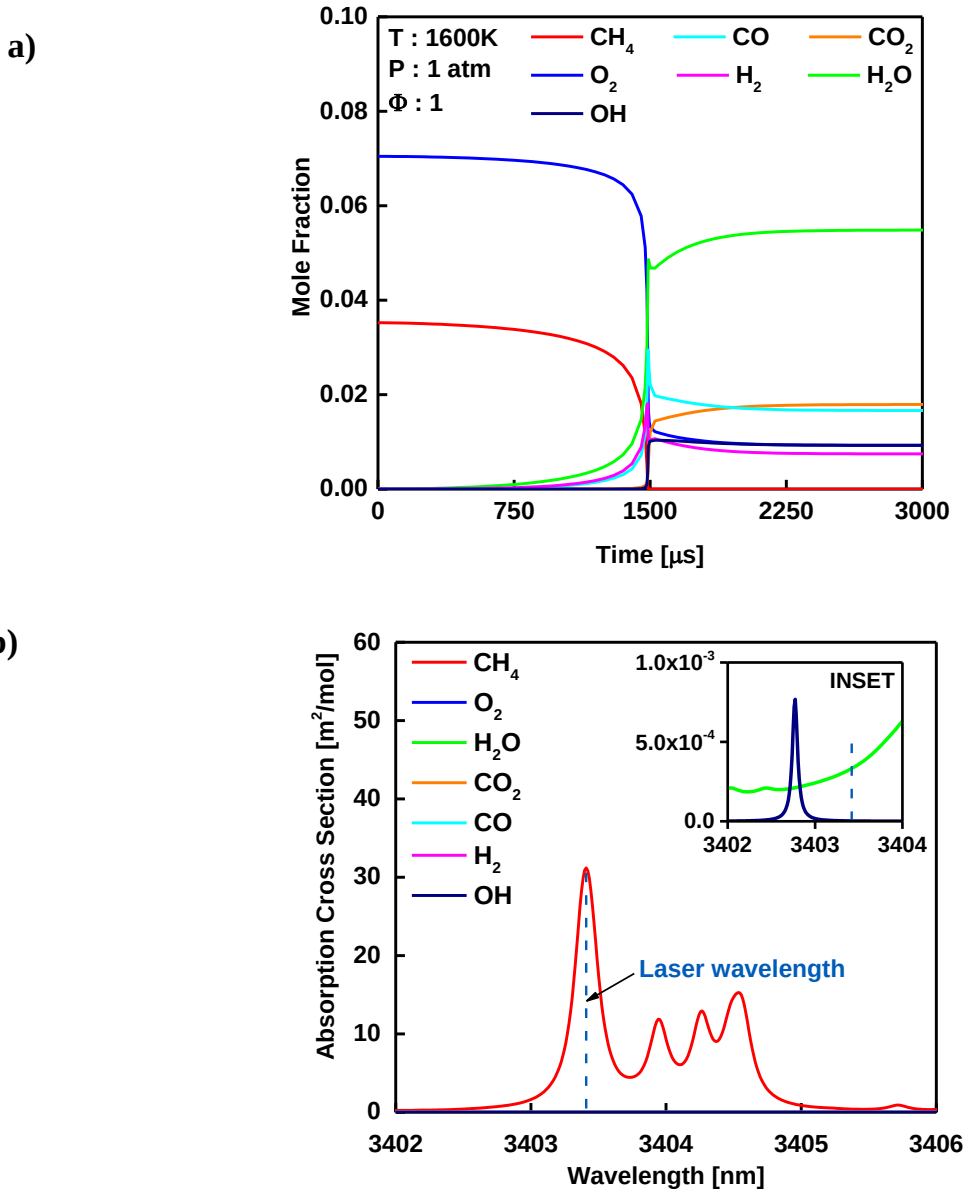

Figure 3 (a) The AramcoMech 1.3 prediction results for the main products of the ignition of 3.5% CH_4 and 7% O_2 in argon at 1600K, 1atm; **(b)** HITRAN [28] absorption cross section values for the main products of the ignition of 3.5% CH_4 and 7% O_2 in argon at 296 K and 1 atm.

3. RESULTS AND DISCUSSION

Table 1 includes a summary of the ignition delay time values obtained in this study behind the reflected shock waves for mixtures of $CH_4/CO_2/O_2$ in argon bath gas at temperatures of 1577 < T < 2144 K, pressures around 1 and 4 atm, equivalence ratios (Φ) of 0.5, 1, and 2, and CO_2 mole fractions (X_{CO2}) of 0, 0.3, and 0.6.

3.1 Methane Ignition without CO_2 Dilution

The pressure and thus the test times required for a shock wave experiment can be estimated from the simulation program KASIMIR 3 [29]. It assumes one dimensional, inviscid flow, and involves equilibrium real-gas effects such as the vibrational excitation. Figure 4 provides the comparison of the measured and simulated pressure for reflected shock conditions of T = 1662 K and P ~ 1.0 atm. The driver and driven gasses were helium and argon, respectively. The experimentally obtained test time was more than 3000 μs, which was sufficient since the ignition delay times measured in the current study were not more than 2500 μs for 1600 < T_5 < 2100 K and 1 < P_5 <4 atm.

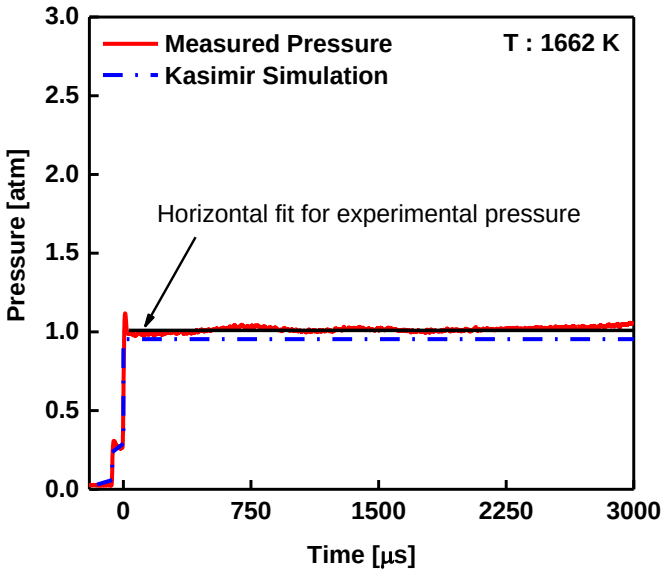

Figure 4 The comparison of measured and KASIMIR simulated pressure for reflected shock conditions of T = 1662 K and P ~ 1.0 atm. The experimental test time was more than 3000 μs. The driver and driven gasses were helium and argon, respectively.

Table 2 Summary of Ignition Delay Time Experimental Data

P_5 [atm]	T_5 [K]	X_{CO2}	X_{CH4}	X_{O2}	X_{AR}	Φ	τ [μs]
0.882	1577						2142.2
0.87	1663						980.5
0.871	1792	0.0	0.035	0.07	0.895	1.0	352.1
0.835	1891						194.9
0.886	2144						38.5
0.818	1737						530.9
0.788	1801						382.3
0.776	1850	0.3	0.035	0.07	0.595	1.0	277.9
0.755	1903						185.2
0.731	1942						157.4
0.684	2022						104
4.038	1660						363.6
3.929	1706						232.0
3.868	1748	0.3	0.035	0.07	0.595	1.0	162.2
3.653	1807						100.1
3.602	1865						59.9
3.544	1904						38.9
0.814	1714						601.4
0.826	1791						370.8
0.829	1837	0.3	0.0175	0.07	0.6125	0.5	269.5
0.766	1846						262.7
0.725	1877						154.0
0.703	2012						90.3
4.104	1610						396.9
4.41	1613						391.7
4.035	1696	0.3	0.0175	0.07	0.6125	0.5	169.3
3.688	1760						105.5
3.722	1848						57.1
3.565	1881						40.5
0.68	1736						758.5
0.716	1812						427.6
0.721	1841						342.9
0.704	1857	0.3	0.07	0.07	0.56	2.0	311.5
0.681	1864						302.7
0.677	1921						190.3
0.615	1962						184.2
3.828	1632						535.2
3.562	1677						382.9
3.792	1684						337.9
3.897	1681	0.3	0.07	0.07	0.56	2.0	323.1
3.462	1736						233.9
3.355	1800						121.3
3.418	1884						52.3
3.288	1896						51.9
0.698	1799						465.9
0.641	1851						330.7
0.603	1960	0.6	0.035	0.07	0.295	1.0	196.4
0.528	2114						92.8
0.567	2091						89.5

The experimental result of the pressure in the reflected shock region matched well with the simulation result obtained from KASIMIR. Due to the boundary layer effects the incident shock wave decelerated (shock attenuation) and the contact surface accelerated which was mainly the reason for the experimental test times being shorter than the simulated ones. Also, since the contact surface is not a sharp discontinuity, multiple pressure waves are reflected at the contact surface as a result of the interaction with the reflected shock wave. This results in a small pressure increase instead of a sharp step as shown by the KASIMIR simulation [29]. Furthermore, the diaphragm rupture and shock formation in reality is not instantaneous as assumed in KASIMIR. However, the horizontal fit shown in Fig. 4 indicates that the nonideal shock tube effects did not cause the experimental pressure to rise dramatically with time ($dP_5/dt \sim 0$) during our tests because of the large diameter of the current shock tube employed (hence minimizing boundary layer influences). Hence driver inserts [30] were not used in the current study.

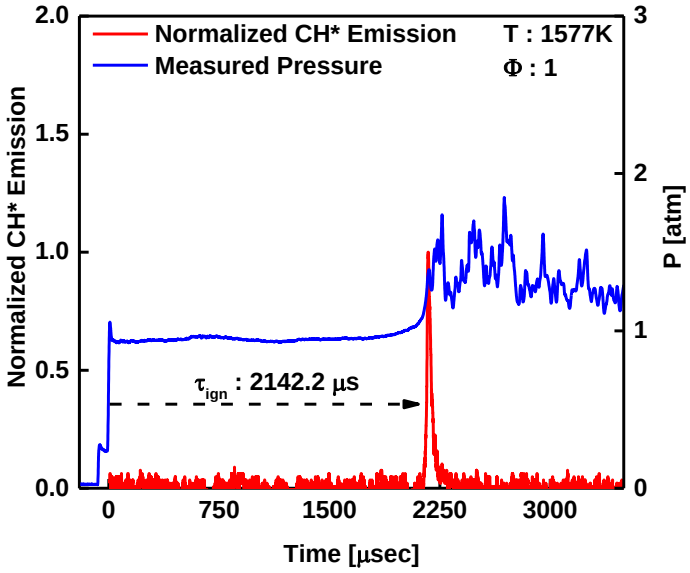

Figure 5 Pressure and normalized CH* emission traces during the ignition of 3.5% CH_4 and 7% O_2 in argon at P_5 ~ 1.0 atm and T_5=1577 K.

Figure 5 shows the pressure and normalized CH* emission traces during the stoichiometric ignition of 3.5% CH_4 in argon at P_5 ~ 1.0 atm and T_5=1577 K. The CH* emission output from the detector was normalized to its peak (maximum) voltage. This approach was suggested by previous studies in the literature [31-33]. It can be clearly seen from Fig. 5 that both the pressure jump and CH* emission peak occur around the same time. In this case, the ignition delay time can be obtained from either the pressure or emission; the discrepancy between them being less than 2%.

The comparison of ignition delay time measurement results of a stoichiometric mixture of 3.5% CH_4 in argon bath gas with GRI 3.0 and AramcoMech 1.3 mechanisms at different temperatures are provided in Fig. 6. The experimental data were obtained behind reflected shock waves between 1577 K

and 2144 K and at P ~ 1.0 atm. The experimental data matched the AramcoMech 1.3 mechanism predictions reasonably well for temperatures between 1600 and 1900 K; however, the GRI predictions were roughly 30% lower than the measured data. Both mechanisms slightly over predicted the ignition delay time above 2000 K. Also, Fig. 6 shows the shock tube ignition delay time measurements of a very recent study conducted by Aul et al. [34] for the stoichiometric ignition of methane at 1 atm in argon bath gas. The agreement between the two experimental measurements were very good especially around 1700 K. There are several other studies in the literature on methane ignition delay times [35-37]; however, the study of Aul et al. was chosen for comparison with present data due to its similarities in pressure, temperature, bath gas, and experimental setup.

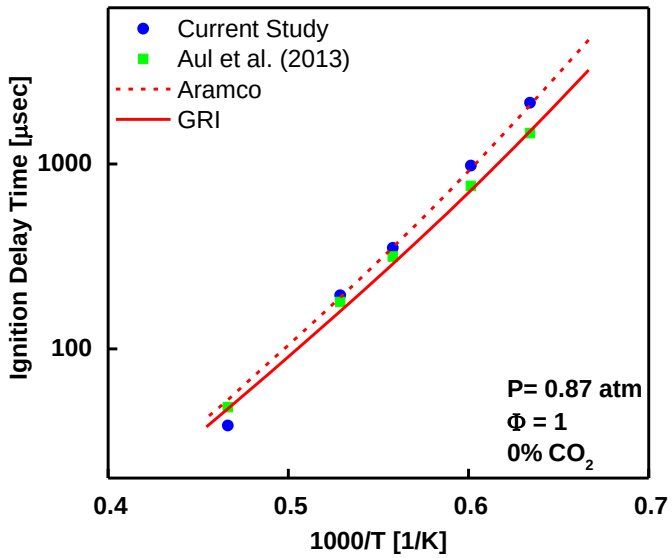

Figure 6 Comparison of measured ignition delay times with shock tube measurements of Aul et al. and predictions of the GRI 3.0 and the AramcoMech 1.3 mechanisms for stoichiometric (3.5% CH_4 and 7% O_2) mixtures in argon at P_5~ 1.0 atm.

In this study, a continuous wave DFB ICL was used to generate light at a peak wavelength in methane's v_3 band, 3403.4 nm. In order to obtain the concentration time-histories of methane, the absorption cross section of methane at elevated temperatures was required. A mixture of 2% CH_4 in argon was used for these measurements. Fig. 7 shows the CH_4 absorption cross section values measured between 1200 < T < 2000 K and 0.9 < P < 1.2 atm. The experimental data were fitted into the following the equation

$$\sigma(T,P) = \sigma_o \left(\frac{T_o}{T}\right)^{2.86} \left(\frac{P_o}{P}\right)^{0.116} \qquad (2)$$

where σ_o = 5.26 m^2/mol, T_o = 1500 K, and P_o = 1 atm.

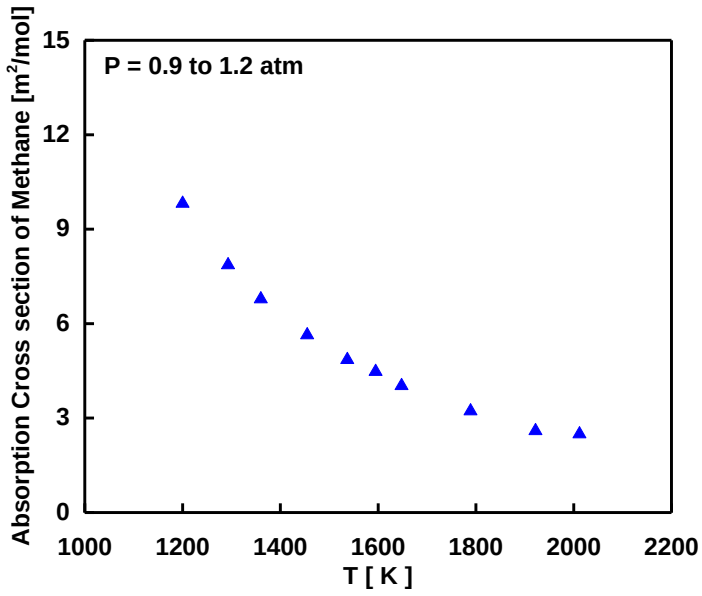

Figure 7 CH_4 absorption cross section values between 1200-2000 K and 0.9-1.2 atm. The results were obtained by using a non-reactive test gas comprised of 2% CH_4 in argon. See [38] for details.

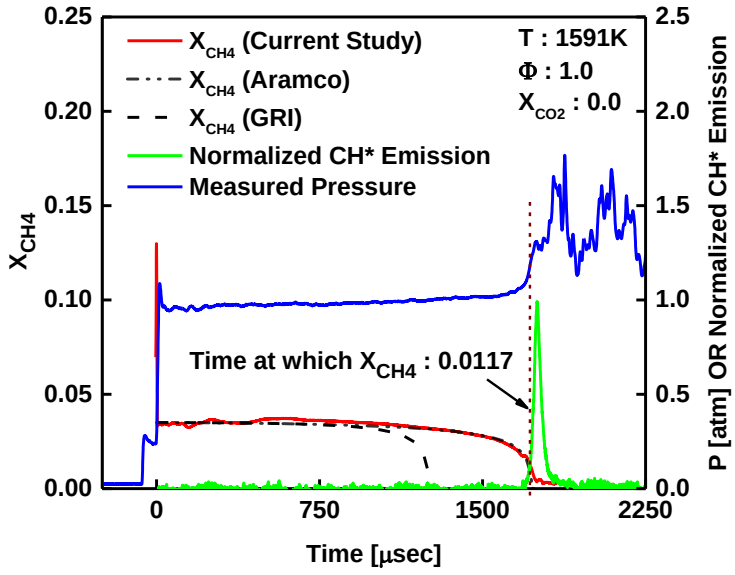

Figure 8 Pressure and CH_4 mole fraction time-histories during the ignition of 3.5% CH_4 and 7% O_2 in argon. The experimental data were obtained at P_5 ~ 1.0 atm and T_5=1591 K.

The correlation given by Eq. (2) was used to obtain the concentration time-histories of methane during its ignition. Figure 8 provides the pressure and CH_4 mole fraction time-histories during the ignition of 3.5% CH_4 and 7% O_2 in argon. The experimental data were obtained behind the reflected shock wave at P_5 ~ 1.0 atm and T_5=1591 K. The steepest rise and fall of the pressure and methane mole fraction traces, respectively, very well matched each other at ignition. Fig. 8 also displays the comparison of the

CH_4 time-histories data with two different mechanism predictions. As shown the measured mole fraction time-histories closely followed the AramcoMech 1.3 mechanism predictions. Also, it can be seen from Fig. 8 that the discrepancy in the ignition delay time at 1591 K between the current study and the AramcoMech 1.3 ($\Delta\tau_{ign}$ = 3 μs) was much less than that of the GRI 3.0 ($\Delta\tau_{ign}$ = 475 μs). Note that in Fig. 8 the measured methane mole fraction (X_{CH4}) values did not cease at zero, which might be due to the absorption of light at 3403.4 nm by water vapor as evidenced by the inset in Fig. 3 (b) or by some other hydrocarbons that were formed as methane depleted before the ignition. However, the current experimental study results very well served for the purpose of confirming the AramcoMech 1.3 mechanism predictions by means of three different measurements: pressure, CH* emission, and CH_4 time-histories. Also, the laser schlieren spike was included in Fig. 8. Due to the arrival of the reflected shock wave at the measurement location, abrupt density gradients occurred and they resulted in changes in the refractive index. As a result, the schlieren spike appeared because of the deflection of the laser beam. Furthermore, Fig. 8 included the time at which methane mole fraction decreased to one-third (X_{CH4} ~ 0.0117) of its initial value (X_{CH4} ~ 0.035). The reason for showing this mole fraction value is explained later in section 3.5.

The study of Pyun et al. [25] gave an empirical correlation for the differential absorption cross section of methane, measured at the peak and valley wavelength pair: λ_{peak} = 3403.4 nm and λ_{valley} = 3403.7 nm, for T=1000-2000 K and P=1.3-5.4 atm. In the current study, measurements of methane concentration time-histories were conducted during its ignition at the aforementioned peak and valley wavelength pair in order to see if the differential measurement could result in the methane mole fraction to cease at zero. The differential absorbance measurements showed complete extinction of methane when the ignition occurred. However, the use of Pyun et al. empirical correlation for these measurements resulted in the initial mole fraction of methane to be off by more than 15%. The reason for this was that the absorption cross section of methane varied significantly due to slight pressure variations and the pressure range of the present study (P ~ 1.0 atm) lied slightly out of the applicable range of the empirical correlation (1.3 < P < 5.4 atm) given by Pyun et al. [25]. In addition, measurements of methane cross section in a CO_2 diluted argon bath gas were done to see the effect of collisional broadening in the absorption cross section of methane. In the literature, there is no study, to the best of our knowledge, giving the absorption cross section of methane measured in a bath gas of CO_2 around 3.4 μm at high temperatures pertinent to combustion. Detailed results [38] for the absorption cross section of methane at the aforementioned peak and valley wavelengths at high temperatures around atmospheric pressures with and without CO_2 dilution are presented elsewhere.

3.2 Methane Ignition with CO_2 Dilution

Provided in Fig. 9 are the pressure and normalized CH* emission traces during the stoichiometric ignition of 3.5% CH_4 in Argon bath gas diluted with 30% CO_2 at P ~ 1.0 atm and T = 1800 K. It can be clearly seen from Fig. 9 that the pressure rise was very gradual for this test mixture involving CO_2. Therefore, the ignition delay time measurements were consistently

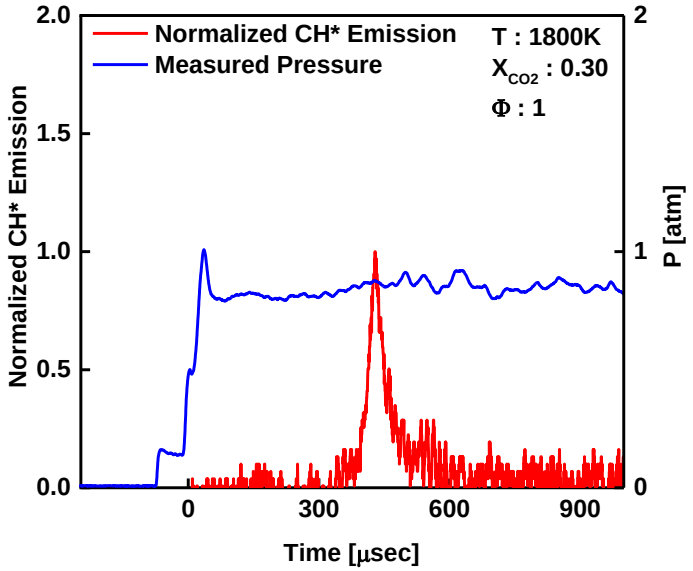

Figure 9 Pressure and normalized CH* emission traces during the ignition of 3.5% CH_4 and 7% O_2 in argon bath gas diluted with 30% CO_2 at P ~ 1.0 atm and T=1800 K.

based off the time interval between the arrival of the shock wave obtained from the pressure trace and the onset of ignition indicated by the CH* emission.

Figure 10 shows the CH_4 absorption cross section values measured between 1400 < T < 2000 K and 0.7 < P < 1.0 atm in argon bath gas diluted with 30% CO_2. The experimental data were fitted into the following the equation

$$\sigma(T,P) = \sigma_o \left(\frac{T_o}{T}\right)^{4.36} \left(\frac{P_o}{P}\right)^{1.95} \qquad (3)$$

where σ_o = 4.93 m^2/mol, T_o = 1500 K, and P_o = 1 atm.

The correlation given by Eq. (3) was used to obtain the concentration time-histories of methane during its ignition in a carbon dioxide diluted mixture. Figure 11 plots the pressure and CH_4 time-histories during the ignition of 3.5% CH_4 and 7% O_2 in argon diluted with 30% CO_2 at P ~ 1.0 atm and T = 1801 K. Also, the comparisons of the experimental data with two different mechanisms predictions are shown. The measured mole fraction time-histories very closely followed the AramcoMech 1.3 mechanism prediction results. Also, it can be seen from Fig. 11 that the discrepancy in the ignition delay time at 1801

K between the current study and the AramcoMech 1.3 was ($\Delta\tau_{ign}$ = 5 μs) much less than that of the GRI 3.0 ($\Delta\tau_{ign}$ = 54 μs).

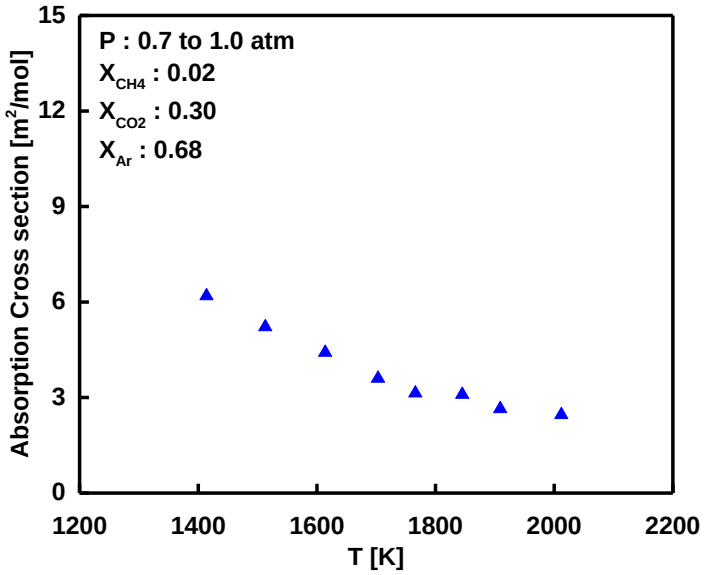

Figure 10 CH_4 absorption cross section values at 1400-2000 K and 0.7-1.0 atm. The results were obtained by using a non-reactive test gas comprised of 2% CH_4+30% CO_2 in argon. See [38] for details.

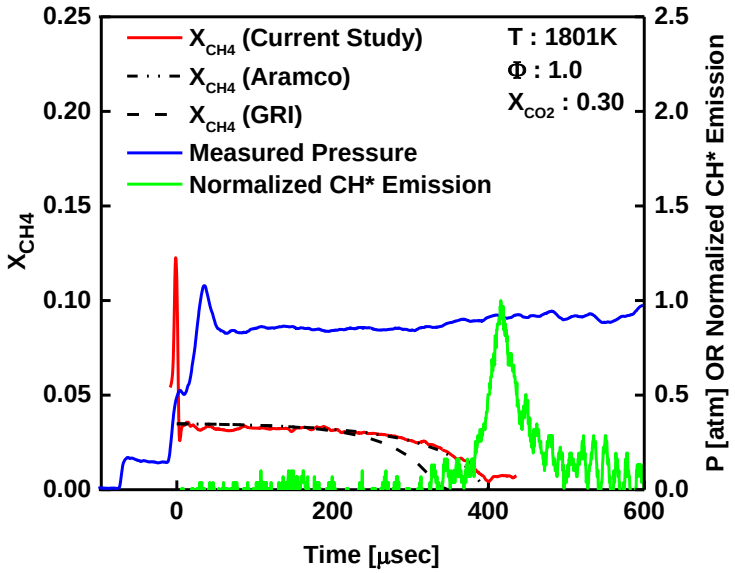

Figure 11 Pressure and CH_4 mole fraction time-histories during the ignition of 3.5% CH_4, 7% O_2, and 30% CO_2 in argon. The experimental data were obtained behind the reflected shock wave at P_5 ~ 1.0 atm and T_5 = 1801 K.

Figure 12 shows the pressure, normalized CH* emission, and absorbance time histories during

the stoichiometric ignition of 3.5% CH_4 in argon bath gas diluted with 60% CO_2 at P ~ 0.60 atm and T = 1960 K. The absorbance trace instead of methane mole fraction was displayed in the figure. The reason was that the measurements of the absorption cross section of CH_4 in 60% CO_2 diluted gas mixtures were not carried out in this study because it was out of the scope of this paper. However, the line of zero absorbance was also given in the figure to indicate the time of depletion of CH_4. The pressure trace included in Fig. 12 exhibited a significant bifurcation feature. The bifurcation seen in the measured pressure profiles of Figs. 11 and 12 occurred because the boundary layer did not have sufficient momentum to pass through the normal reflected shock wave. The possibility of bifurcation increases with the amount of di-atomic/polyatomic molecules in the test gas mixture [39]. The severity of the bifurcation also increases as the γ (specific heat ratio) of the gas decreases. Therefore, the measured pressure profiles in Figs. 11 and 12 showed bifurcation since the gas mixtures involved 30 and 60% CO_2 (γ_{CO2} = 1.28), whereas no bifurcation was observed in Fig. 5 due to the use of un-diluted monatomic bath gas Ar (γ_{Ar}=1.66). Owing to the same reasons, the pressure trace displayed a much stronger bifurcation in Fig. 12 than that in Fig. 11. Similarly, it was realized that the laser schlieren spikes illustrated in Fig. 12 had higher peaks than those given in Figs. 5 and 11. However, the temporal width of the schlieren spikes were very similar for all three cases; namely, 0, 30, and 60 % CO_2 diluted gas mixtures. Thus the schlieren spikes indicated the arrival of the main reflected shock wave at the test location as detailed below.

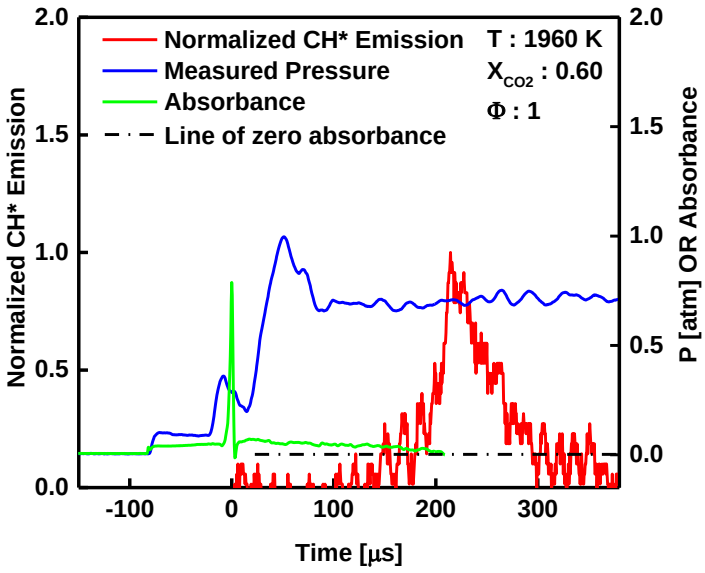

Figure 12 Pressure, normalized CH* emission, and the absorbance time histories during the ignition of 3.5% CH_4, 7% O_2, and 60% CO_2 in argon. The experimental data were obtained behind the reflected shock wave at P_5 ~ 0.65 atm and T_5 = 1960 K. The line of zero absorbance is also shown in the figure to indicate the time of depletion of CH_4 from the laser measurements.

When the bifurcation happens, the arrival of the main reflected shock wave (i.e. time zero)

becomes questionable. However, Petersen and Hanson [40] pointed out that the arrival of the normal portion of the reflected shock wave can be accurately determined using a laser diagnostic that outputs a continuous wave (cw) beam. In fact, they provided experimentally obtained correlations based on the laser measurements to figure out the time zero from a side wall pressure measurement, if pressure is the only form of data available in a shock tube experiment. Since the current study made use of a cw laser source, the time zero was based off the peak schlieren spike during the ignition delay time measurements for CO_2 diluted gas mixtures. The bifurcation also leads to concerns regarding the non-ideal effects due the boundary layer build up. However, the core section of the post-shock region consists of most of the flow area as discussed in [40] and therefore this portion still has the gasses at the calculated T_5 and P_5. As a result, the measured ignition delay time should not be altered due to the existence of a bifurcation feature as long as the ignition occurs at a temporal location in which the calculated P_5 (through shock velocity measurements) matches the measured P_5 (through Kistler pressure transducer). In other words, if the ignition delay time is to be accurately determined, the ignition should happen after the bifurcation is passed over (which is the case in our present study).

a)

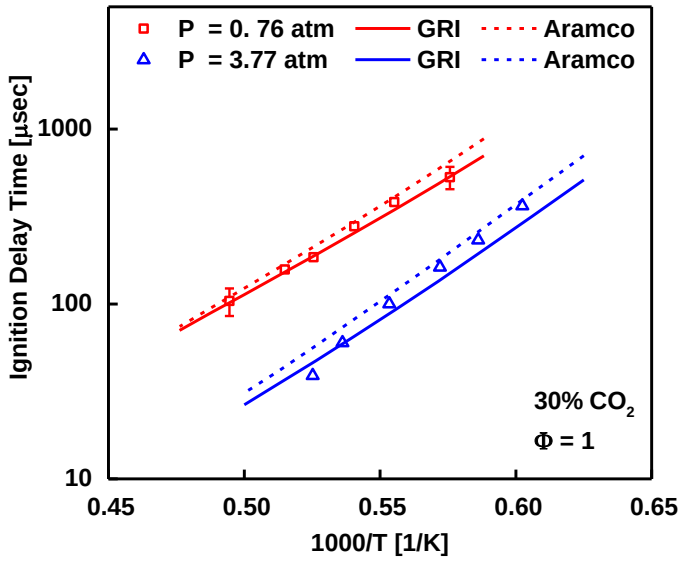

b)

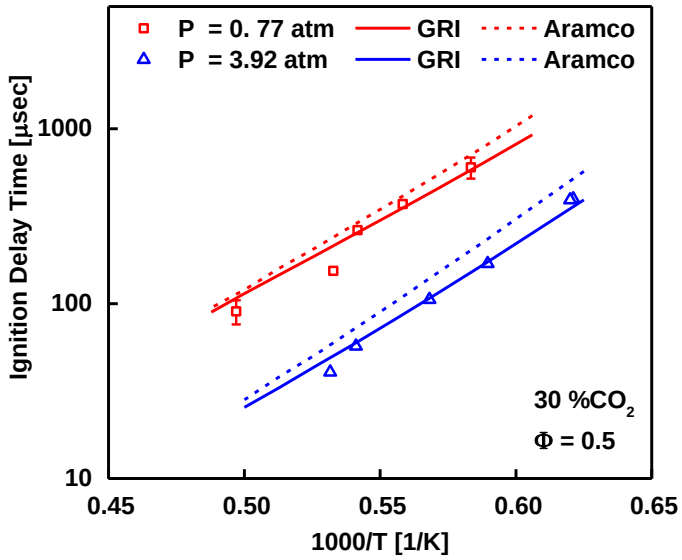
P = 0. 77 atm
GRI
Aramco
P = 3.92 atm
GRI
Aramco
Ignition Delay Time [µsec]
1000
100
10
0.45
0.50
0.55
0.60
0.65
1000/T [1/K]
30 %CO2
Φ = 0.5

c)

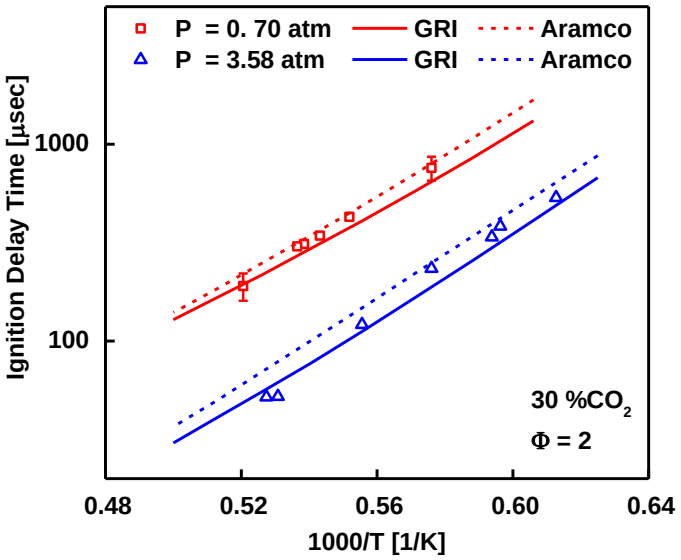
P = 0. 70 atm
GRI
Aramco
P = 3.58 atm
GRI
Aramco
Ignition Delay Time [µsec]
1000
100
0.48
0.52
0.56
0.60
0.64
1000/T [1/K]
30 %CO2
Φ = 2

d)

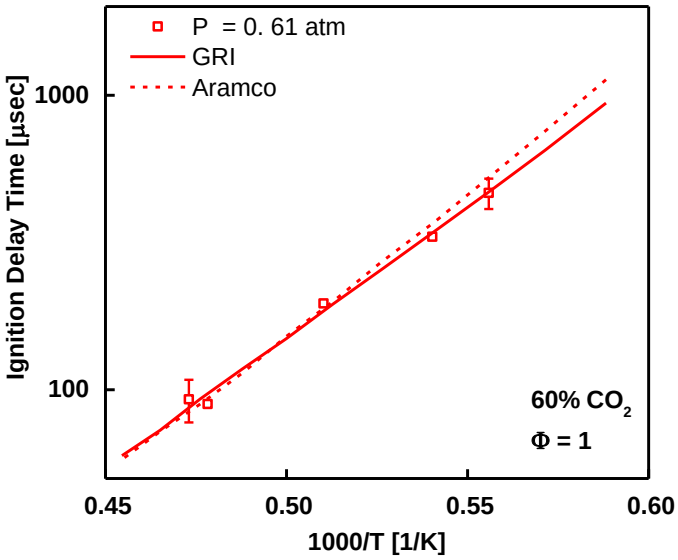

Figure 13 Comparison of ignition delay time data with GRI 3.0 and AramcoMech 1.3 mechanisms at different pressures around 1 and 4 atm for equivalence ratios of **(a)** 30%CO_2, Φ = 1, **(b)** 30%CO_2, Φ = 0.5, **(c)** 30%CO_2, Φ =2, and (**d)** 60%CO_2, Φ =1.

The comparison of ignition delay time measurements results from emission traces with the predictions of GRI 3.0 and AramcoMech 1.3 mechanisms at two different pressures around 1 and 4 atm, with 30% and 60% CO_2 dilution of the bath gas, for three different equivalence ratios: Φ = 1**,** Φ = 0.5, and Φ = 2 are shown in Fig. 13. Figure 13 (a) results were obtained by using 3.5% CH_4, 7% O_2, and 30% CO_2 in argon. It can be seen that the GRI 3.0 mechanism reproduced the activation energy better than the AramcoMech 1.3 predictions at low pressures. However, both mechanisms underpredicted the activation energy at high pressures. Also, at high pressures the simulation results obtained from AramcoMech 1.3 better matched the current study results at low temperatures, whereas the GRI 3.0 mechanism estimates had a smaller deviation from the experimental results at higher temperatures. Figure 13 (b) results were gathered from 1.75% CH_4, 7% O_2, and 30% CO_2 in argon. GRI 3.0 mechanism exhibited better agreement with regards to the activation energy and ignition delay time at both pressures in this case. Figure 13 (c) compares results achieved by using 7% CH_4, 7% O_2, and 30% CO_2 in argon. The ignition delay time values of the present study at both pressures lied within the predictions of two mechanisms, however, the activation energies were underpredicted by both mechanisms. Figure 13 (d) shows ignition delay time results obtained from 3.5% CH_4, 7% O_2, and 60% CO_2 in argon. GRI 3.0 mechanism exhibited better agreement with regards to the activation energy and ignition delay time. In general it could be said that both mechanisms are able to reasonably predict the data taken in current experiments with high CO_2 dilution.

3.3 Empirical Correlations for the Current Experimental Data

The experimental data were fitted into the following form of the correlation

$$\tau = Ae^{E/RT} P^b \phi^c X_{CO2}{}^d \tag{4}$$

where the ignition delay times are in μs, temperatures are in K, pressures are in atm, and the activation energy is in kcal/mole. Using all the data taken with CO_2 diluted gas mixtures, the following empirical relation was obtained

$$\tau = 8.11x10^{-4}(\pm 2.50x10^{-4}) e^{46.83\pm 1.10/RT} P^{-0.75\pm 0.021} \phi^{0.22\pm 0.020} X_{CO2}{}^{0.21\pm 0.058} \tag{5}$$

where the statistical uncertainties of the correlation parameters are also included. The curve fit represented the experimental data with a correlation coefficient greater than $R^2 > 0.98$. In order to better illustrate the effect of CO_2 dilution on the ignition delay time, the experimentally obtained correlation parameter, b, shown in Eq. (4) and given in Eq. (5) was utilized to scale the ignition delay time data to P = 1 atm as follows

$$\tau_{scaled} = \tau_{original}(1/P)^b \tag{6}$$

Figure 14 shows the scaled ignition delay time results. The scaling was implemented on the ignition delay time data taken at stoichiometric conditions (Φ =1) for three different CO_2 dilution percentages (X_{CO2} = 0, 0.3, and 0.6). For this data set, Table 1 showed that there were slight variations in pressure between 0.528 < P < 0.886 atm. The scaled results of Fig. 15 pointed out the very slight increases of ignition delay time as X_{CO2} was increased. When X_{CO2} was raised from 0 to 0.3, the increase in ignition delay time was very small (~10%) around 2000 K, whereas it became somewhat bigger (~25%) when X_{CO2} was further raised to 0.6. Similarly, the differences were small (~15%) at lower temperatures. Therefore, it can be concluded that the changes in the ignition delay time of methane after CO_2 addition to the argon bath gas are within the experimental uncertainties.

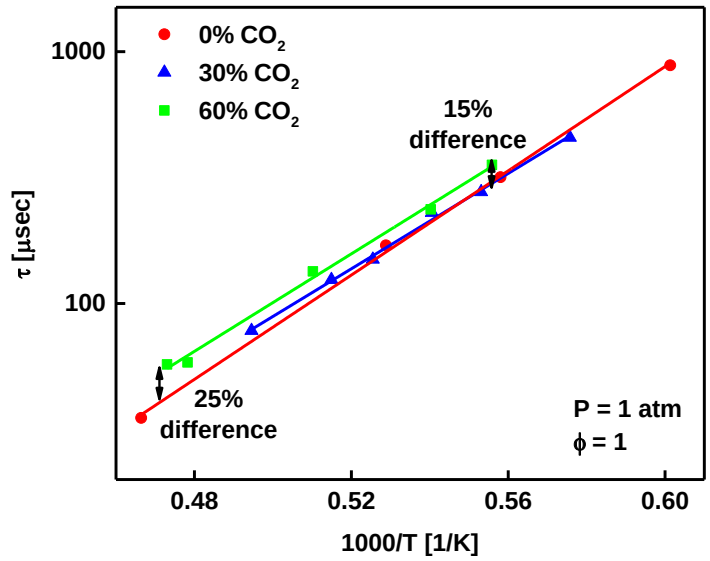

Figure 14 Comparison of scaled ignition delay time measurement results at 0, 30, and 60 % CO_2 dilutions. The results were scaled to 1 atm at stoichiometric conditions.

3.4 Chemical and Thermodynamic Effects of CO_2 Addition

A brute force sensitivity analysis [21, 41, 42] for ignition delay time was carried out for the experimental result obtained at 1737 K and 0.818 atm for stoichiometric ignition of 3.5% CH_4 in argon bath gas diluted with 30% CO_2. It was seen that the most dominant reaction in the system was the chain branching reaction as expected:

$$R_1 : H + O_2 \rightarrow O + OH$$

, whereas the seventh most dominant reaction was

$$R_2 : CO + OH \rightarrow CO_2 + H$$

It has been clearly mentioned in a previous study by Liu et al. [5] that CO_2 is not an inert bath gas in the ignition of CH_4 and H_2 premixed flames. In fact, CO_2 competes for the H radicals through the reverse reaction of R_2, which results in a decrease in the concentration of the H radicals that participates in the chain branching reaction given by R_1. As a result, the fuel (CH_4) burning rate decreases as well. The current experimental results support this conclusion since ignition of methane in CO_2 diluted bath gas leads to longer ignition delay times.

a)

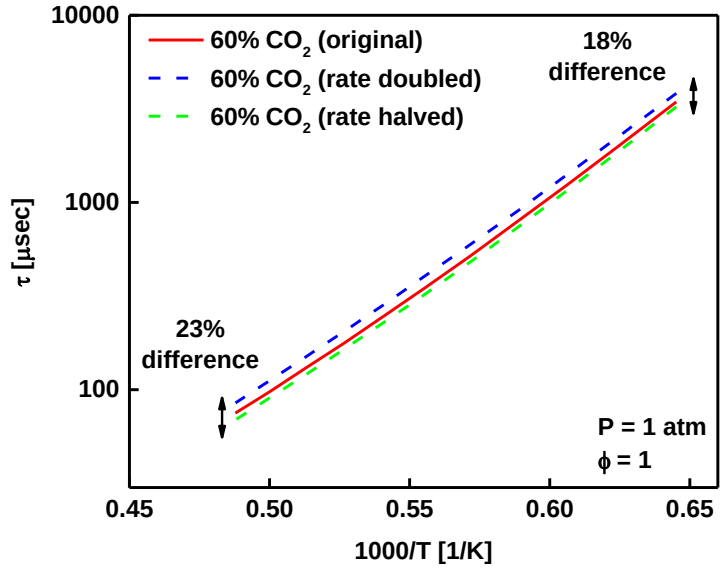

b)

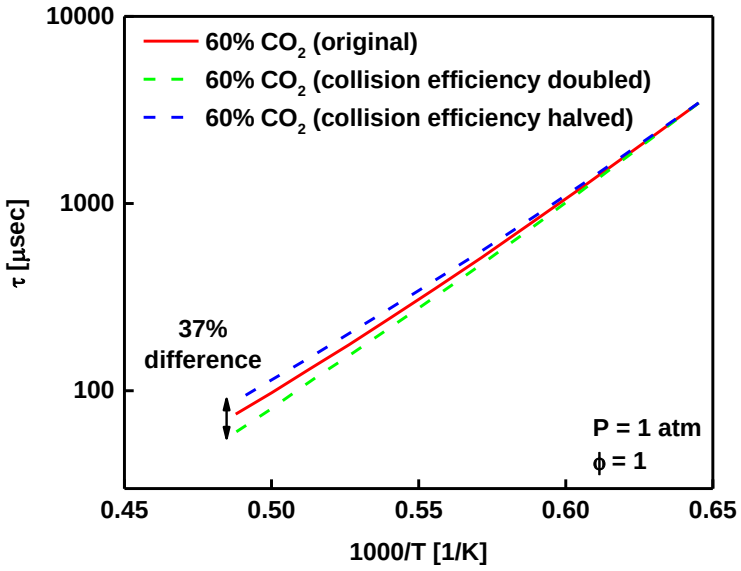

Figure 15 The variations in ignition delay time as a result of changing the (a) reaction rate of R_2 and (b) third body collision efficiencies of CO_2. The simulations were carried out using the AramcoMech 1.3 mechanism for the stoichiometric combustion of CH_4 at 1 atm with 60 % CO_2 dilution.

There are mainly three influences of CO_2 addition on the ignition delay time of methane: 1) CO_2 can participate in chemical reactions through one of the most dominant reaction in the system which is R_2, 2) CO_2 has different third body collision efficiencies (α) in comparison to Argon or N_2; and 3) CO_2 exhibits a much higher heat capacity (c_p) than argon and N_2. The reaction rate of R_2 was determined by

Joshi and Wang through RRKM/master equation analyses and Monte Carlo simulations [43]. In the present study, this reaction rate was doubled and halved in the AramcoMech 1.3 mechanism and the resulting ignition delay time results were compared to the original ones in Fig. 16 (a). The simulations were done for stoichiometric combustion of 3.5% CH_4 in argon bath gas diluted with 60% CO_2 at 1 atm. The variation in ignition delay time due to the change in reaction rate of R_2 was insignificant with differences being slightly larger at higher temperatures. In addition, a similar ignition delay time comparison was carried out and shown in Fig. 16 (b) by changing the collision efficiencies of CO_2. The original AramcoMech 1.3 mechanism had collision efficiencies (when compared to nitrogen) of CO_2 lying between 1.6 and 3.8 (average of them being $\alpha_{CO2} \sim 2.2$) for 29 different reactions, whereas these values were between 0.7 and 0.83 for argon (average of them being $\alpha_{Ar} \sim 0.71$). An ignition delay time comparison with the collision efficiencies of CO_2 doubled and halved was displayed in Fig. 16 (b). When the collision efficiencies were varied, no change was noticed at low temperatures close to 1600 K, whereas somewhat larger differences (~ 37%) in the ignition delay time were seen at higher temperatures near 2000 K. Furthermore, the heat capacity of CO_2 ($c_{p,CO2}$ = 1.357 kJ/kgK) was almost three times higher than that of argon ($c_{p,Ar}$ = 0.52 kJ/kgK) above 1600 K. However, this difference manifested itself as a smaller pressure and thus temperature variation after ignition, when large amounts of CO_2 were employed in the gas mixture. This was evident by the large pressure fluctuations shown in Figs. 5 and 8 for the 0% CO_2 dilution case, whereas a much smaller change in pressure was observed in Figs. 9 and 11 and Fig. 12 for the 30 and 60% CO_2 diluted gas mixtures, respectively.

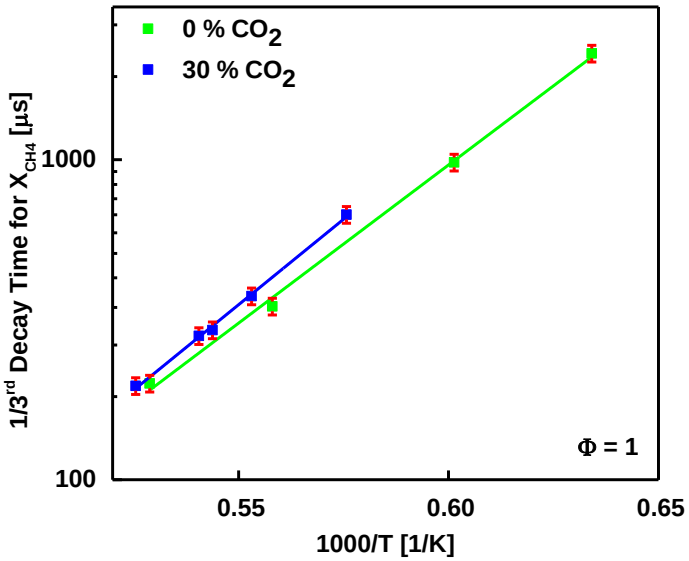

Figure 16 The laser absorption data for the initial CH_4 mole fraction ($X_{CH4} \sim 0.0350$) to fall to one-third of its initial value ($X_{CH4} \sim 0.0117$) for two different CO_2 dilutions (0 and 30%) at 1atm.

3.5 Methane Concentration Decay Times

Based on Eq. (1) there is uncertainty in the calculation of absorption cross section and mole fraction due to the errors in the measurements of pressure, temperature, absorbance, and path length. A very similar uncertainty analysis was already detailed elsewhere [44] and followed in this study. The resulting uncertainties of the current study were determined to be ±4 and ±6% for methane absorption cross section and mole fraction, respectively. The laser intensity fluctuations were also accounted for in this analysis. Similar uncertainties were reported for methane concentration measurements via laser absorption spectroscopy using similar types of DFB laser diodes in the infrared region [45]. The uncertainties in methane mole fraction measurements were much smaller than those of the ignition delay time measurements. Therefore, a time scale measurement scheme according to the methane mole fraction decay was adopted in order to make a better comparison between data taken at different CO_2 dilutions. To accomplish that, the time that it takes for the initial methane mole fraction ($X_{CH4} = 0.035$) to decrease to one-third of its initial value ($X_{CH4} = 0.0117$) was plotted for different temperatures in Fig. 16 for 0 and 30% CO_2 diluted gas mixtures. Recall that this time value was already exemplified in Fig. 8. The increase in time for the methane mole fraction to decay as the CO_2 dilution was raised from 0 to 30% was 20% around 1740 K. Thus using the measured CH_4 time profiles, it can be said that addition of CO_2 causes a delay in CH_4 decay. It should be noted that in the present study addition of CO_2 replacement caused the ignition delay time to increase slightly, which were within the uncertainties of the ignition delay time measurements. The CH_4 mole fraction measurements aided in resolving this minor increase, because the mole fraction measurement uncertainties were much less than those of the ignition delay time measurements.

4. CONCLUSIONS

In this study we provided shock tube ignition delay time measurements for mixtures of CH_4, CO_2 and O_2 in argon bath gas at temperatures of $1577 < T < 2144$ K, pressures around 1 and 4 atm, equivalence ratios (Φ) of 0.5, 1, and 2, and CO_2 mole fractions (X_{CO2}) of 0, 0.3, and 0.6. Methane concentration, CH* emission, and pressure time-histories measurements were conducted behind reflected shock waves to gain insight into the effects of CO_2 dilution on the ignition delay time of methane combustion. Current experiments are the first shock tube ignition experiments with excess CO_2 dilution ($\geq$ 30%) for methane combustion in argon. Empirical correlations were obtained for ignition of methane at different CO_2 dilution percentages. The results pointed out that the changes in the methane ignition delay times as a result of CO_2 addition to the argon bath gas were not significant enough to be resolved in terms of the uncertainty of the ignition delay time measurements. However, the mole fraction traces had smaller uncertainties and thus helped gain insight into the changes in the methane decay time as the CO_2

dilution was increased. Also, the results were compared to the predictions of two different models: GRI 3.0 and AramcoMech 1.3 mechanisms. Both mechanisms were able to predict current data reasonably well with the AramcoMech 1.3 predictions in better agreement. Sensitivity analysis was carried out to understand the important reactions. Three different influences in regards to chemistry, collision efficiencies, and heat capacities were examined as a result of CO_2 addition into the gas mixtures. The chemistry and global collision efficiency effects were found to be negligibly small to alter the ignition delay time of methane for the experimental conditions of interest. In addition, the present study included experimentally obtained correlations for absorption cross sections of methane for its P(8) line in the v_3 band (λ = 3403.4 nm) in argon bath gas with and without carbon-dioxide dilutions at temperatures of $1200 < T < 2000$ K and pressures of $0.7 < P < 1.2$ atm. Efforts are currently underway in our lab to extend the current study to higher pressures and increased CO_2 dilution.

Acknowledgements

Research at UCF was mainly supported by financial assistance from Mechanical and Aerospace Department, Florida Space Institute, and the Office of Research and Commercialization. Donors of the American Chemical Society Petroleum Research Fund and the Department of Energy (grant number: DE-FE0025260) are acknowledged for the partial financial support. J.L. thanks the UCF RAMP program.

5. REFERENCES

1. Annual Energy Outlook 2014. 2014 [cited 2015; Available from: http://www.eia.gov/forecasts/aeo/pdf/0383(2014).pdf.
2. X. Hu, Q. Yu, J. Liu, and N. Sun, Investigation of laminar flame speeds of CH4/O2/CO2 mixtures at ordinary pressure and kinetic simulation, Energy 70 (2014) 626-634.
3. P. Heil, D. Toporov, M. Förster, and R. Kneer, Experimental investigation on the effect of O2 and CO2 on burning rates during oxyfuel combustion of methane, Proc. Combust. Inst. 33(2) (2011) 3407-3413.
4. A. Di Benedetto, F. Cammarota, V. Di Sarli, E. Salzano, and G. Russo, Reconsidering the flammability diagram for CH4/O2/N2 and CH4/O2/CO2 mixtures in light of combustion-induced Rapid Phase Transition, Chem. Eng. Sci. 84 (2012) 142-147.
5. F. Liu, H. Guo, and G.J. Smallwood, The chemical effect of CO2 replacement of N2 in air on the burning velocity of CH4 and H2 premixed flames, Combust. Flame 133(4) (2003) 495-497.
6. A.A. Konnov and I.V. Dyakov, Measurement of propagation speeds in adiabatic cellular premixed flames of CH4+O2+CO2, Exp. Therm Fluid Sci. 29(8) (2005) 901-907.
7. A. Mazas, D.A. Lacoste, and T. Schuller. Experimental and numerical investigation on the laminar flame speed of CH4/O2 mixtures diluted with CO2 and H2O, Proc. of the ASME Turbo Expo 2010: Power for Land, Sea, and Air (2010), paper GT2010-22512.
8. S. de Persis, F. Foucher, L. Pillier, V. Osorio, and I. Gökalp, Effects of O2 enrichment and CO2 dilution on laminar methane flames, Energy 55 (2013) 1055-1066.
9. B. Almansour, J. Lopez, L. Thompson, G. Barari, and S.S. Vasu, Ignition and Flame Propagation in Oxy-Methane Mixtures Diluted with CO2, Proc. of the ASME Turbo Expo (2015), paper GT2015-43355.
10. S.S. Vasu, D.F. Davidson, and R.K. Hanson, Shock tube study of syngas ignition in rich CO2 mixtures and determination of the rate of H+ O2+ CO2→ HO2+ CO2, Energy Fuels 25(3) (2011) 990-997.
11. M. Holton, P. Gokulakrishnan, M. Klassen, R. Roby, and G. Jackson, Autoignition delay time measurements of methane, ethane, and propane pure fuels and methane-based fuel blends, Journal of Engineering for Gas Turbines and Power 132(9) (2010) 091502.
12. G.P. Smith, D.M. Golden, M. Frenklach, N.W. Moriarty, B. Eiteneer, M. Goldenberg, C.T. Bowman, R.K. Hanson, S. Song, and W.C. Gardiner Jr, GRI-Mech 3.0. (1999).
13. W.K. Metcalfe, S.M. Burke, S.S. Ahmed, and H.J. Curran, A Hierarchical and Comparative Kinetic Modeling Study of C1 − C2 Hydrocarbon and Oxygenated Fuels, Int. J. Chem. Kinet. 45(10) (2013) 638-675.
14. CHEMKIN-PRO 15131. 2013, Reactiondesign: San Diego, CA.
15. S.S. Vasu and S.M. Sarathy, On the high-temperature combustion of n-butanol: Shock tube data and an improved kinetic model accepted, Energy Fuels 27(11) (2013) 7072-7080.
16. S.S. Vasu, L.K. Huynh, D.F. Davidson, R.K. Hanson, and D.M. Golden, Reactions of OH with Butene Isomers: Measurements of the Overall Rates and a Theoretical Study, J. Phys. Chem. A 115(12) (2011) 2549-2556.
17. S.S. Vasu, J. Zádor, D.F. Davidson, R.K. Hanson, D.M. Golden, and J.A. Miller, High-Temperature Measurements and a Theoretical Study of the Reaction of OH with 1,3-Butadiene, J. Phys. Chem. A. 114 (2010) 8312-8318.
18. S.S. Vasu, Z. Hong, D.F. Davidson, R.K. Hanson, and D.M. Golden, Shock Tube/Laser Absorption Measurements of the Reaction Rates of OH with Ethylene and Propene, J. Phys. Chem. A. 114(43) (2010) 11529-11537.
19. S.S. Vasu, D.F. Davidson, R.K. Hanson, and D.M. Golden, Measurements of the reaction of OH with n-butanol at high-temperatures, Chem. Phys. Letters 497 (2010) 26.
20. Z. Hong, S.S. Vasu, D.F. Davidson, and R.K. Hanson, Experimental study of the rate of OH+ HO2→ H2O+ O2 at high temperatures using the reverse reaction, J. Phys. Chem. A 114 (2010) 5520-5525.
21. S.S. Vasu, D.F. Davidson, Z. Hong, and R.K. Hanson, Shock Tube Study of Methylcyclohexane Ignition over a Wide Range of Pressure and Temperature, Energy Fuels 23 (2009) 175-185.
22. A.G. Gaydon and I.R. Hurle, The Shock Tube in High-Temperature Chemical Physics, Reinhold, New York, 1963.
23. S.S. Vasu, D.F. Davidson, and R.K. Hanson, Jet fuel ignition delay times: Shock tube experiments over wide conditions and surrogate model predictions, Combust. Flame 152(1-2) (2008) 125-143.
24. A.S. Pine, Self-, N2, O2, H2, Ar, and He broadening in the ν3 band Q branch of CH4, J. Chem. Phys. 97(2) (1992) 773-785.

25. S.H. Pyun, J. Cho, D.F. Davidson, and R.K. Hanson, Interference-free mid-IR laser absorption detection of methane, Meas. Sci. Technol. 22 (2011) 025303.
26. S.H. Pyun, W. Ren, D.F. Davidson, and R.K. Hanson, Methane and ethylene time-history measurements in n-butane and n-heptane pyrolysis behind reflected shock waves, Fuel 108(0) (2013) 557-564.
27. K. Y. Lam, W. Ren, S.H. Pyun, A. Farooq, D.F. Davidson, and R.K. Hanson, Multi-species time-history measurements during high-temperature acetone and 2-butanone pyrolysis, Proc. Combust. Inst. 34(1) (2013) 607-615.
28. L.S. Rothman, I.E. Gordon, Y. Babikov, A. Barbe, D. Chris Benner, P.F. Bernath, M. Birk, L. Bizzocchi, V. Boudon, L.R. Brown, A. Campargue, K. Chance, E.A. Cohen, L.H. Coudert, V.M. Devi, B.J. Drouin, A. Fayt, J.M. Flaud, R.R. Gamache, J.J. Harrison, J.M. Hartmann, C. Hill, J.T. Hodges, D. Jacquemart, A. Jolly, J. Lamouroux, R.J. Le Roy, G. Li, D.A. Long, O.M. Lyulin, C.J. Mackie, S.T. Massie, S. Mikhailenko, H.S.P. Müller, O.V. Naumenko, A.V. Nikitin, J. Orphal, V. Perevalov, A. Perrin, E.R. Polovtseva, C. Richard, M.A.H. Smith, E. Starikova, K. Sung, S. Tashkun, J. Tennyson, G.C. Toon, V.G. Tyuterev, and G. Wagner, The HITRAN2012 molecular spectroscopic database, J. Quant. Spectrosc. Radiat. Transfer 130 (2013) 4-50.
29. K.A. Heufer and H. Olivier, Determination of ignition delay times of different hydrocarbons in a new high pressure shock tube, Shock Waves 20(4) (2010) 307-316.
30. Z. Hong, G.A. Pang, S.S. Vasu, D.F. Davidson, and R.K. Hanson, The use of driver inserts to reduce non-ideal pressure variations behind reflected shock waves, Shock Waves 19 (2009) 113-123.
31. K. Chatelain, R. Mével, S. Menon, G. Blanquart, and J.E. Shepherd, Ignition and chemical kinetics of acrolein–oxygen–argon mixtures behind reflected shock waves, Fuel 135(0) (2014) 498-508.
32. J.M. Hall, M.J.A. Rickard, and E.L. Petersen, Comparison Of Characteristic Time Diagnostics For Ignition And Oxidation Of Fuel/Oxidizer Mixtures Behind Reflected Shock Waves, Combust. Sci. Technol. 177(3) (2005) 455-483.
33. M. Kopp, M. Brower, O. Mathieu, E. Petersen, and F. Güthe, CO2* chemiluminescence study at low and elevated pressures, Appl. Phys. B 107(3) (2012) 529-538.
34. C.J. Aul, W.K. Metcalfe, S.M. Burke, H.J. Curran, and E.L. Petersen, Ignition and kinetic modeling of methane and ethane fuel blends with oxygen: A design of experiments approach, Combust. Flame 160(7) (2013) 1153-1167.
35. A. Lifshitz, K. Scheller, A. Burcat, and G.B. Skinner, Shock-tube investigation of ignition in methane-oxygen-argon mixtures, Combust. Flame 16(3) (1971) 311-321.
36. N. Lamoureux, C.E. Paillard, and V. Vaslier, Low hydrocarbon mixtures ignition delay times investigation behind reflected shock waves, Shock Waves 11(4) (2002) 309-322.
37. V.P. Zhukov, V.A. Sechenov, and A.Y. Starikovskii, Spontaneous Ignition of Methane–Air Mixtures in a Wide Range of Pressures, Combustion, Explosion and Shock Waves 39(5) (2003) 487-495.
38. B. Koroglu, O.M. Pryor, J. Lopez, L. Nash, and S.S. Vasu, High Temperature Absorption Cross Sections of Methane near 3.4 μm in Carbon-dioxide Diluted Gas Mixtures, Chem. Phys. Lett. (2015) in review.
39. R.A. Strehlow and A. Cohen, Limitations of the Reflected Shock Technique for Studying Fast Chemical Reactions and Its Application to the Observation of Relaxation in Nitrogen and Oxygen, J. Chem. Phys. 30(1) (1959) 257-265.
40. E.L. Petersen and R.K. Hanson, Measurement of Reflected-shock Bifurcation Over a Wide Range of Gas Composition and Pressure, Shock Waves 16(5) (2006) 333-340.
41. S.S. Vasu, D.F. Davidson, and R.K. Hanson, Shock-Tube Experiments and Kinetic Modeling of Toluene Ignition, J. Prop. Power 26(4) (2010) 776-783.
42. S.S. Vasu, D.F. Davidson, Z. Hong, V. Vasudevan, and R.K. Hanson, n-Dodecane oxidation at high-pressures: Measurements of ignition delay times and OH concentration time-histories, Proc. Combust. Inst. 32 (2009) 173.
43. A.V. Joshi and H. Wang, Master equation modeling of wide range temperature and pressure dependence of CO + OH → products, Int. J. Chem. Kinet. 38(1) (2006) 57-73.
44. B. Koroglu, Z. Loparo, J. Nath, R.E. Peale, and S.S. Vasu, Propionaldehyde infrared cross-sections and band strengths, J. Quant. Spectrosc. Radiat. Transfer 152(0) (2015) 107-113.
45. R. Sur, S. Wang, K. Sun, D.F. Davidson, J.B. Jeffries, and R.K. Hanson, High-sensitivity interference-free diagnostic for measurement of methane in shock tubes, J. Quant. Spectrosc. Radiat. Transfer 156 (2015) 80-87.